

Free Vibration Analysis of a Circular Plate With Multiple Circular Holes by Using Indirect BIEM and Addition Theorem

W. M. Lee

Department of Mechanical Engineering,
China University of Science and Technology,
Taipei, 11581, Taiwan
e-mail: wmllee@cc.cust.edu.tw

J. T. Chen¹

Department of Harbor and River Engineering,
Department of Mechanical and Mechatronic
Engineering,
National Taiwan Ocean University,
Keelung, 20224, Taiwan
e-mail: jtchen@mail.ntou.edu.tw

In this paper, natural frequencies and natural modes of a circular plate with multiple circular holes are theoretically derived and numerically determined by using the indirect boundary integral formulation, the addition theorem, and the complex Fourier series. Owing to the addition theorem, all kernel functions are expanded into degenerate forms and further expressed in the same polar coordinates centered at one circle where the boundary conditions are specified. Not only the computation of the principal value is avoided but also the calculation of higher-order derivatives can be easily determined. By matching boundary conditions, a coupled infinite system of linear algebraic equations is derived as an analytical model for the free vibration of a circular plate with multiple circular holes. The direct-searching approach is utilized in the truncated finite system to determine the natural frequency through singular value decomposition. After determining the unknown Fourier coefficients, the corresponding mode shapes are obtained by using the indirect boundary integral formulations. Some numerical eigensolutions are presented and then utilized to explain some physical phenomenon such as the beating and the dynamic stress concentration. Good accuracy and fast rate of convergence are the main features of the present method, thanks to the analytical approach.

[DOI: 10.1115/1.4001993]

1 Introduction

Circular plates with multiple circular holes are commonly observed in engineering structures [1], e.g., aviation, aerospace, and shipping, either to reduce the weight of the whole structure, to increase the range of inspection, or to satisfy some other engineering designs. In addition, the title problem includes annular-like plates, which are common elements in the rotating machinery with practical applications including disk brake system, circular saw blades, and hard disk for data storage [2]. Geometric discontinuities due to these holes inevitably cause the change in dynamic characteristics as well as the decrease in load carrying capacity. It is important to comprehend the associated effects in the work of the mechanical design or the associated controller design. As stated by Leissa and Narita [3]: "The free vibrations of circular plates have been of practical and academic interest for at least a century and a half." We revisit this problem by proposing a semi-analytical approach.

Over the past few decades, much research has focused on the analytical solutions for natural frequencies of the circular or annular plates [4–7]. Recently, some researchers intended to extend the analysis of an annular plate [8,9] to that of the plate with an eccentric hole. Cheng et al. [8] encountered difficulty and resorted to the finite element method (FEM) to implement the vibration analysis of annular-like plates due to the complicated expression for this kind of plate. Laura et al. [9] determined the natural frequencies of a circular plate with an eccentric hole by using the Rayleigh–Ritz variational method where the assumed function does not satisfy the natural boundary condition in the inner free edge. Lee et al. [10] proposed a semi-analytical approach to solve

the free vibration analysis of a circular plate with multiple holes by using the indirect boundary integral equation method (BIEM).

It is well known that the boundary element method (BEM) or the BIEM can reduce the dimension of the original problem by one, and thus the number of the introduced unknowns is much less than that of the traditional domain type methods such as finite difference method (FDM) or FEM. For BEM applications to plate problems, readers may consult with the review article [11]. By using the BIEM to analytically solve the problem of plate with multiple holes, two problems need to be solved. One is the improper integral in the boundary integral equation; the other is that the field point and the source point locate on different circular boundaries when considering the multiply connected domain problem. These problems have been treated by using the degenerate kernel and tensor transformation [10], respectively. However, tensor transformation accompanied with the higher-order derivative, such as the computation of effective shear force, increases the complexity of computation and then deteriorates the accuracy of its solution. In addition, the collocation method in Ref. [10] belongs to the point-matching approach instead of the analytical derivation. It also increases the effort of computation since boundary nodes for collocation are required to satisfy the pointwise boundary conditions.

This paper presents an analytical model for the free vibration analysis of a circular plate with multiple circular holes by using the indirect boundary integral formulation, addition theorem, and complex Fourier series. When considering a circular plate with multiple circular holes in the indirect boundary integral formulation, the transverse displacement field is represented by all adaptive coordinates centered at each center of circles. By using the addition theorem, it is transformed into the same coordinate centered at the corresponding circle, where the boundary conditions are specified. By this way, the higher derivative such as bending moments and effective shear forces can be easily determined. According to the specified boundary conditions, a coupled infinite system of simultaneous linear algebraic equations is obtained.

¹Corresponding author.

Contributed by the Applied Mechanics of ASME for publication in the JOURNAL OF APPLIED MECHANICS. Manuscript received April 28, 2009; final manuscript received March 13, 2010; accepted manuscript posted June 16, 2010; published online October 22, 2010. Assoc. Editor: Subrata Mukherjee.

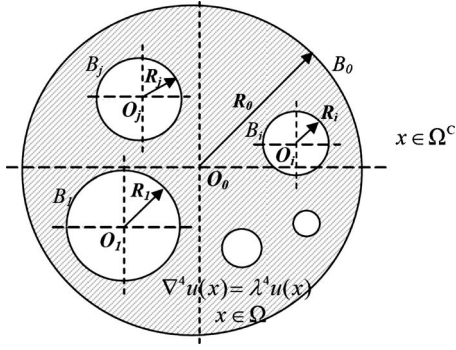


Fig. 1 Problem statement for an eigenproblem of a circular plate with multiple circular holes

Based on the direct-searching approach [12], the nontrivial eigen-solution can be determined by finding the zero determinant of the truncated finite system through singular value decomposition (SVD) [13]. Several numerical examples are presented, and the proposed results of a circular plate with an eccentric circular hole and multiple circular holes are compared with those of semi-analytical solutions [10], global discretization method [2], and FEM using the ABAQUS [14]. The results of eigensolution for the plate with two holes can be used to explain the reason why the dynamic concentration occurs when two holes are close to each other.

2 Problem Statement and Indirect Boundary Integral Formulation

2.1 Problem Statement of Plate Eigenproblem. A uniform thin circular plate with H nonoverlapping circular holes centered at the position vector O_k ($k=0, 1, \dots, H$; O_0 is the position vector of the outer circular boundary of the plate) has a domain Ω , which is enclosed with boundary

$$B = \bigcup_{k=0}^H B_k \quad (1)$$

as shown in Fig. 1, where R_k and B_k denote the radius and the boundary of the k th circle, respectively. The governing equation of the free flexural vibration for this plate is expressed as

$$\nabla^4 u(x) = \lambda^4 u(x), \quad x \in \Omega \quad (2)$$

where ∇^4 is the biharmonic operator, u is the lateral displacement, $\lambda^4 = \omega^2 \rho_0 h / D$, λ is the frequency parameter, ω is the circular frequency, ρ_0 is the volume density, h is the plate thickness, $D = Eh^3 / 12(1 - \mu^2)$ is the flexural rigidity of the plate, E denotes the Young's modulus, and μ is the Poisson's ratio

2.2 Indirect Boundary Integral Formulation. Based on the indirect boundary integral formulation, the displacement field of plate vibration can be represented by [15]

$$u(x) = \int_B P(s, x) \phi(s) dB(s) + \int_B Q(s, x) \psi(s) dB(s), \quad x \in \Omega \quad (3)$$

where B is the boundary of the domain Ω , s and x mean the source and field points, respectively, $\phi(s)$ and $\psi(s)$ are the unknown fictitious density distributions on the boundary, $P(s, x)$ and $Q(s, x)$ are kernel functions, which can be chosen from any two of the four kernel functions, U , Θ , M , and V , which will be elaborated on later. The kernel function $U(s, x)$ is the fundamental solution, which satisfies

$$\nabla^4 U(s, x) - \lambda^4 U(s, x) = \delta(s - x) \quad (4)$$

where $\delta(s - x)$ is the Dirac-delta function. Considering the two singular solutions ($Y_0(\lambda r)$ and $K_0(\lambda r)$, which are the zeroth order of the second-kind Bessel and modified Bessel functions, respectively) and one regular solution ($J_0(\lambda r)$ is the zeroth order of the first-kind Bessel function) in the fundamental solution, we have the complex-valued kernel [12],

$$U(s, x) = \frac{1}{8\lambda^2 D} \left[Y_0(\lambda r) - iJ_0(\lambda r) + \frac{2}{\pi} K_0(\lambda r) \right] \quad (5)$$

where $r = |s - x|$ and $i^2 = -1$. The other three kernels, $\Theta(s, x)$, $M(s, x)$, and $V(s, x)$ can be obtained by applying the following slope, moment, and effective shear operators defined by

$$K_\Theta = \frac{\partial(\cdot)}{\partial n} \quad (6)$$

$$K_M = -D \left[\mu \nabla^2(\cdot) + (1 - \mu) \frac{\partial^2(\cdot)}{\partial n^2} \right] \quad (7)$$

$$K_V = -D \left[\frac{\partial}{\partial n} \nabla^2(\cdot) + (1 - \mu) \frac{\partial}{\partial t} \left(\frac{\partial}{\partial n} \left(\frac{\partial}{\partial t}(\cdot) \right) \right) \right] \quad (8)$$

to the kernel $U(s, x)$ with respect to the source point, where $\partial/\partial n$ and $\partial/\partial t$ are the normal and tangential derivatives, respectively; ∇^2 means the Laplacian operator. In the polar coordinates of (R, γ) , the normal and tangential derivatives can be expressed by $\partial/\partial R$ and $(1/R) \partial/\partial \gamma$, respectively, and then the three kernel functions can be rewritten as

$$\Theta(s, x) = K_{\Theta, s}(U(s, x)) = \frac{\partial U(s, x)}{\partial R} \quad (9)$$

$$M(s, x) = K_{M, s}(U(s, x)) = -D \left[\mu \nabla_s^2 U(s, x) + (1 - \mu) \frac{\partial^2 U(s, x)}{\partial R^2} \right] \quad (10)$$

$$V(s, x) = K_{V, s}(U(s, x)) = -D \left[\frac{\partial}{\partial R} (\nabla_s^2 U(s, x)) + (1 - \mu) \times \left(\frac{1}{R} \right) \frac{\partial}{\partial \gamma} \left(\frac{\partial}{\partial R} \left(\frac{1}{R} \frac{\partial U(s, x)}{\partial \gamma} \right) \right) \right] \quad (11)$$

Since the kernels $P(s, x)$ and $Q(s, x)$ can be selected from any two of the four kernels, $U(s, x)$, $\Theta(s, x)$, $M(s, x)$, and $V(s, x)$, six (C_2^4) formulations can be considered. For the computational efficiency, the kernels $U(s, x)$ and $\Theta(s, x)$ are chosen as $P(s, x)$ and $Q(s, x)$ in Eq. (3). In addition to the displacement, the slope, the normal moment, and the effective shear force are derived by applying the three operators in Eqs. (6)–(8) to Eq. (3) with respect to the field point as follows:

$$u(x) = \int_B U(s, x) \phi(s) dB(s) + \int_B \Theta(s, x) \psi(s) dB(s), \quad x \in \Omega \quad (12)$$

$$\theta(x) = \int_B U_\theta(s, x) \phi(s) dB(s) + \int_B \Theta_\theta(s, x) \psi(s) dB(s), \quad x \in \Omega \quad (13)$$

$$m(x) = \int_B U_m(s, x) \phi(s) dB(s) + \int_B \Theta_m(s, x) \psi(s) dB(s), \quad x \in \Omega \quad (14)$$

$$v(x) = \int_B U_v(s, x) \phi(s) dB(s) + \int_B \Theta_v(s, x) \psi(s) dB(s), \quad x \in \Omega \quad (15)$$

For the clamped case, the lateral displacement $u(x)$ and the slope $\theta(x)$ on the boundary are specified to be zero. For the free case, the normal moment $m(x)$ and the effective shear force $v(x)$ on the boundary are set to be zero. The simply supported

condition can be obtained by specifying both the lateral displacement $u(x)$ and the normal moment $m(x)$ to be zero.

2.3 Degenerate Kernels and Complex Fourier Series for the Fictitious Boundary Densities. In the polar coordinates, the field point and source point can be expressed as $x=(\rho, \phi)$ and $s=(R, \gamma)$, respectively. By using the addition theorem [16], the kernel functions $U(s, x)$ and $\Theta(s, x)$ are expanded in the series form as follows:

$$U: \begin{cases} U^I(s, x) = \frac{1}{8\lambda^2 D} \sum_{m=-\infty}^{\infty} \left\{ J_m(\lambda \rho) [Y_m(\lambda R) - iJ_m(\lambda R)] + \frac{2}{\pi} I_m(\lambda \rho) K_m(\lambda R) \right\} e^{im(\phi-\gamma)}, & \rho < R \\ U^E(s, x) = \frac{1}{8\lambda^2 D} \sum_{m=-\infty}^{\infty} \left\{ J_m(\lambda R) [Y_m(\lambda \rho) - iJ_m(\lambda \rho)] + \frac{2}{\pi} I_m(\lambda R) K_m(\lambda \rho) \right\} e^{im(\phi-\gamma)}, & \rho \geq R \end{cases} \quad (16)$$

$$\Theta: \begin{cases} \Theta^I(s, x) = \frac{1}{8\lambda D} \sum_{m=-\infty}^{\infty} \left\{ J_m(\lambda \rho) [Y'_m(\lambda R) - iJ'_m(\lambda R)] + \frac{2}{\pi} I_m(\lambda \rho) K'_m(\lambda R) \right\} e^{im(\phi-\gamma)}, & \rho < R \\ \Theta^E(s, x) = \frac{1}{8\lambda D} \sum_{m=-\infty}^{\infty} \left\{ J'_m(\lambda R) [Y_m(\lambda \rho) - iJ_m(\lambda \rho)] + \frac{2}{\pi} I'_m(\lambda R) K_m(\lambda \rho) \right\} e^{im(\phi-\gamma)}, & \rho > R \end{cases} \quad (17)$$

where the superscripts I and E denote the interior and exterior cases for $U(s, x)$ degenerate kernel to distinguish $\rho < R$ and $\rho > R$, respectively, as shown in Fig. 2. The other degenerate kernels $U_\theta(s, x)$, $\Theta_\theta(s, x)$, $U_m(s, x)$, $\Theta_m(s, x)$, $U_v(s, x)$, and $\Theta_v(s, x)$ in the indirect boundary integral equations can be obtained by applying the operators of Eqs. (6)–(8) to the degenerate kernel $U(s, x)$ and $\Theta(s, x)$ in Eqs. (16) and (17) with respect to the field point x . In order to fully utilize the geometry of circular boundary, the fictitious boundary densities, $\phi(s)$ and $\psi(s)$, can be expanded by employing the complex Fourier series as follows:

$$\phi^k(s) = \sum_{n=-\infty}^{\infty} a_n^k e^{in\gamma_k}, \quad s \in B_k, \quad k=0, \dots, H \quad (18)$$

$$\psi^k(s) = \sum_{n=-\infty}^{\infty} b_n^k e^{in\gamma_k}, \quad s \in B_k, \quad k=0, \dots, H \quad (19)$$

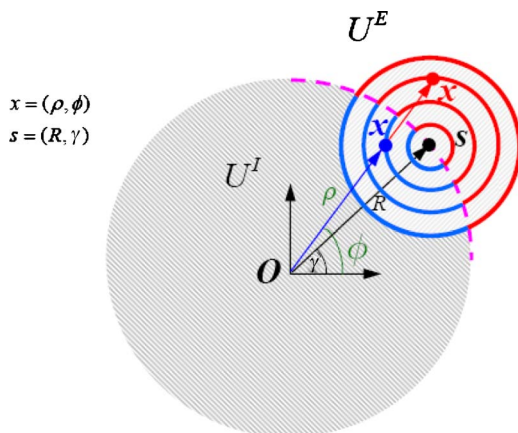


Fig. 2 Degenerate kernel for $U(s, x)$

where a_n^k and b_n^k are the complex Fourier coefficients of the k th circular boundary, γ_k is its polar angle and H is the number of inner holes.

3 Eigensolutions for a Circular Plate With Multiple Circular Holes

Considering a circular plate with H circular holes, Eq. (12) can be explicitly expressed as

$$u(x) = \int_{B_0} U^I(s_0, x) \phi(s_0) dB_0(s_0) + \int_{B_0} \Theta^I(s_0, x) \psi(s_0) dB_0(s_0) - \left[\sum_{k=1}^H \int_{B_k} U^E(s_k, x) \phi(s_k) dB_k(s_k) + \int_{B_k} \Theta^E(s_k, x) \psi(s_k) dB_k(s_k) \right], \quad x \in \Omega \quad (20)$$

Substituting both the degenerate kernels, Eqs. (16) and (17), and the fictitious boundary densities, Eqs. (18) and (19), into Eq. (20) in the adaptive coordinate system, we have

$$\begin{aligned} u(x; \rho_0, \phi_0, \rho_1, \phi_1, \dots, \rho_H, \phi_H) &= \int_{B_0} \left(\frac{1}{8\lambda^2 D} \sum_{m=-\infty}^{\infty} \left\{ J_m(\lambda \rho_0) [Y_m(\lambda R_0) - iJ_m(\lambda R_0)] + \frac{2}{\pi} I_m(\lambda \rho_0) K_m(\lambda R_0) \right\} e^{im(\phi_0-\gamma_0)} \right) \left(\sum_{n=-\infty}^{\infty} a_n^0 e^{in\gamma_0} \right) dB_0(s_0) \\ &+ \int_{B_0} \left(\frac{1}{8\lambda D} \sum_{m=-\infty}^{\infty} \left\{ J_m(\lambda \rho_0) [Y'_m(\lambda R_0) - iJ'_m(\lambda R_0)] + \frac{2}{\pi} I_m(\lambda \rho_0) K'_m(\lambda R_0) \right\} e^{im(\phi_0-\gamma_0)} \right) \left(\sum_{n=-\infty}^{\infty} b_n^0 e^{in\gamma_0} \right) dB_0(s_0) \end{aligned}$$

$$\begin{aligned}
& - \sum_{k=1}^H \left[\int_{B_k} \left(\frac{1}{8\lambda^2 D} \sum_{m=-\infty}^{\infty} \left\{ J_m(\lambda R_k) [Y_m(\lambda \rho_k) - iJ_m(\lambda \rho_k)] \right. \right. \right. \\
& \left. \left. \left. + \frac{2}{\pi} I_m(\lambda R_k) K_m(\lambda \rho_k) \right\} e^{im(\phi_k - \gamma_k)} \right) \left(\sum_{n=-\infty}^{\infty} a_n^k e^{in\gamma_k} \right) dB_k(s_k) \right. \\
& \left. + \int_{B_k} \frac{1}{8\lambda D} \sum_{m=-\infty}^{\infty} \left\{ J'_m(\lambda R_k) [Y_m(\lambda \rho_k) - iJ_m(\lambda \rho_k)] \right. \right. \\
& \left. \left. \left. + \frac{2}{\pi} I'_m(\lambda R_k) K_m(\lambda \rho_k) \right\} e^{im(\phi_k - \gamma_k)} \left(\sum_{n=-\infty}^{\infty} b_n^k e^{in\gamma_k} \right) dB_k(s_k) \right] \quad (21)
\end{aligned}$$

where the $(\rho_0, \phi_0), (\rho_1, \phi_1), \dots, (\rho_H, \phi_H)$ are the polar coordinates of the field point x in the local coordinates at the center of the corresponding circle. By employing the analytical integration along each circular boundary in the adaptive coordinate and by applying the orthogonal property, Eq. (21) can be rewritten as

$$\begin{aligned}
& u(x; \rho_0, \phi_0, \rho_1, \phi_1, \dots, \rho_H, \phi_H) \\
& = \frac{\pi R_0}{4\lambda^2 D} \sum_{m=-\infty}^{\infty} \left\{ J_m(\lambda \rho_0) [Y_m(\lambda R_0) - iJ_m(\lambda R_0)] \right. \\
& \left. + \frac{2}{\pi} I_m(\lambda \rho_0) K_m(\lambda R_0) \right\} a_m^0 e^{im\phi_0} + \frac{\pi R_0}{4\lambda D} \sum_{m=-\infty}^{\infty} \left\{ J_m(\lambda \rho_0) [Y'_m(\lambda R_0) \right. \\
& \left. - iJ'_m(\lambda R_0)] + \frac{2}{\pi} I_m(\lambda \rho_0) K'_m(\lambda R_0) \right\} b_m^0 e^{im\phi_0} \\
& - \sum_{k=1}^H \left[\frac{\pi R_k}{4\lambda^2 D} \sum_{m=-\infty}^{\infty} \left\{ J_m(\lambda R_k) [Y_m(\lambda \rho_k) - iJ_m(\lambda \rho_k)] \right. \right. \\
& \left. \left. + \frac{2}{\pi} I_m(\lambda R_k) K_m(\lambda \rho_k) \right\} a_m^k e^{im\phi_k} + \frac{\pi R_k}{4\lambda D} \sum_{m=-\infty}^{\infty} \left\{ J'_m(\lambda R_k) [Y_m(\lambda \rho_k) \right. \right. \\
& \left. \left. - iJ'_m(\lambda \rho_k)] + \frac{2}{\pi} I'_m(\lambda R_k) K_m(\lambda \rho_k) \right\} b_m^k e^{im\phi_k} \right] \quad (22)
\end{aligned}$$

To determine these unknown coefficients, the other three Eqs. (13)–(15) are required by applying three operators of Eqs. (9)–(11) to Eq. (22). First, this procedure involves the higher-order derivatives. Second, Eq. (22) consists of several different variables. It is difficult to directly derive the formulation. Consequently, it is necessary to transform Eq. (22) into one coordinate system by applying again the addition theorem.

Based on Graf's addition theorem for the Bessel functions given in Refs. [16,17], we can express the theorem in the following form:

$$J_m(\lambda \rho_k) e^{im\phi_k} = \sum_{n=-\infty}^{\infty} J_{m-n}(\lambda r_{kp}) e^{i(m-n)\theta_{kp}} J_n(\lambda \rho_p) e^{in\phi_p} \quad (23)$$

$$I_m(\lambda \rho_k) e^{im\phi_k} = \sum_{n=-\infty}^{\infty} I_{m-n}(\lambda r_{kp}) e^{i(m-n)\theta_{kp}} I_n(\lambda \rho_p) e^{in\phi_p} \quad (24)$$

$$\begin{aligned}
& Y_m(\lambda \rho_k) e^{im\phi_k} \\
& = \begin{cases} \sum_{n=-\infty}^{\infty} Y_{m-n}(\lambda r_{kp}) e^{i(m-n)\theta_{kp}} J_n(\lambda \rho_p) e^{in\phi_p}, & \rho_p < r_{kp} \\ \sum_{n=-\infty}^{\infty} J_{m-n}(\lambda r_{kp}) e^{i(m-n)\theta_{kp}} Y_n(\lambda \rho_p) e^{in\phi_p}, & \rho_p > r_{kp} \end{cases} \quad (25)
\end{aligned}$$

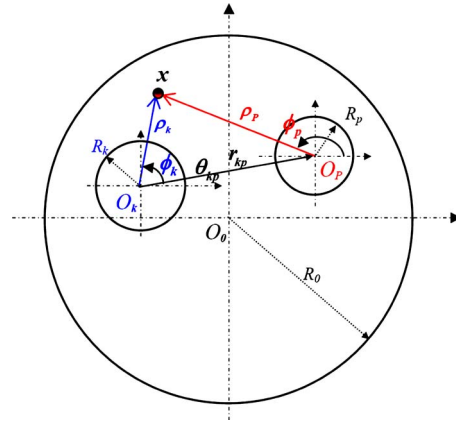


Fig. 3 Notation of Graf's addition theorem for Bessel functions

$$\begin{aligned}
& K_m(\lambda \rho_k) e^{im\phi_k} \\
& = \begin{cases} \sum_{n=-\infty}^{\infty} (-1)^n K_{m-n}(\lambda r_{kp}) e^{i(m-n)\theta_{kp}} I_n(\lambda \rho_p) e^{in\phi_p}, & \rho_p < r_{kp} \\ \sum_{n=-\infty}^{\infty} (-1)^{m-n} I_{m-n}(\lambda r_{kp}) e^{i(m-n)\theta_{kp}} K_n(\lambda \rho_p) e^{in\phi_p}, & \rho_p > r_{kp} \end{cases} \quad (26)
\end{aligned}$$

where (ρ_p, ϕ_p) and (ρ_k, ϕ_k) in Fig. 3 are the polar coordinates of a general field point x with respect to O_p and O_k , which are the origins of two polar coordinate systems, and (r_{kp}, θ_{kp}) are the polar coordinates of O_p with respect to O_k .

By using the addition theorem for the Bessel functions $J_m(\lambda \rho_k)$, $Y_m(\lambda \rho_k)$, and $K_m(\lambda \rho_k)$, the displacement field near the circular boundary B_0 under the condition of $\rho_0 > r_{k0}$ can be expanded as follows:

$$\begin{aligned}
& u(x; \rho_0, \phi_0) \\
& = \frac{\pi R_0}{4\lambda^2 D} \sum_{m=-\infty}^{\infty} \left\{ J_m(\lambda \rho_0) [Y_m(\lambda R_0) - iJ_m(\lambda R_0)] \right. \\
& \left. + \frac{2}{\pi} I_m(\lambda \rho_0) K_m(\lambda R_0) \right\} a_m^0 e^{im\phi_0} \\
& + \frac{\pi R_0}{4\lambda D} \sum_{m=-\infty}^{\infty} \left\{ J_m(\lambda \rho_0) [Y'_m(\lambda R_0) - iJ'_m(\lambda R_0)] \right. \\
& \left. + \frac{2}{\pi} I_m(\lambda \rho_0) K'_m(\lambda R_0) \right\} b_m^0 e^{im\phi_0} \\
& - \sum_{k=1}^H \left[\frac{\pi R_k}{4\lambda^2 D} \sum_{m=-\infty}^{\infty} \left\{ J_m(\lambda R_k) \sum_{n=-\infty}^{\infty} J_{m-n}(\lambda r_{k0}) e^{i(m-n)\theta_{k0}} [Y_n(\lambda \rho_0) \right. \right. \\
& \left. \left. - iJ_n(\lambda \rho_0)] \right. \right. \\
& \left. + \frac{2}{\pi} I_m(\lambda R_k) \sum_{n=-\infty}^{\infty} (-1)^{m-n} I_{m-n}(\lambda r_{k0}) e^{i(m-n)\theta_{k0}} K_n(\lambda \rho_0) \right\} e^{in\phi_0} a_m^k \\
& + \frac{\pi R_k}{4\lambda D} \sum_{m=-\infty}^{\infty} \left\{ J'_m(\lambda R_k) \sum_{n=-\infty}^{\infty} J_{m-n}(\lambda r_{k0}) e^{i(m-n)\theta_{k0}} [Y_n(\lambda \rho_0) \right. \\
& \left. - iJ_n(\lambda \rho_0)] \right. \\
& \left. + \frac{2}{\pi} I'_m(\lambda R_k) \sum_{n=-\infty}^{\infty} (-1)^{m-n} I_{m-n}(\lambda r_{k0}) \right.
\end{aligned}$$

$$\times e^{i(m-n)\theta_{k0}} K_n(\lambda \rho_0) \left\{ e^{in\phi_0} b_m^k \right\} \quad (27)$$

Furthermore, Eq. (27) can be rewritten as

$$u(x; \rho_0, \phi_0) = \sum_{m=-\infty}^{\infty} e^{im\phi_0} \left\langle A_m^0(\lambda \rho_0) a_m^0 + B_m^0(\lambda \rho_0) b_m^0 - \sum_{k=1}^H \left[\sum_{n=-\infty}^{\infty} A_{mn}^k(\lambda \rho_0) a_n^k + \sum_{n=-\infty}^{\infty} B_{mn}^k(\lambda \rho_0) b_n^k \right] \right\rangle \quad (28)$$

where

$$A_m^0(\lambda \rho_0) = \frac{\pi R_0}{4\lambda^2 D} \left\{ J_m(\lambda \rho_0) [Y_m(\lambda R_0) - iJ_m(\lambda R_0)] + \frac{2}{\pi} I_m(\lambda \rho_0) K_m(\lambda R_0) \right\} \quad (29)$$

$$B_m^0(\lambda \rho_0) = \frac{\pi R_0}{4\lambda D} \left\{ J_m(\lambda \rho_0) [Y'_m(\lambda R_0) - iJ'_m(\lambda R_0)] + \frac{2}{\pi} I_m(\lambda \rho_0) K'_m(\lambda R_0) \right\} \quad (30)$$

$$A_{mn}^0(\lambda \rho_0) = \frac{\pi R_k}{4\lambda^2 D} e^{i(n-m)\theta_{k0}} \left\{ J_{n-m}(\lambda r_{k0}) J_n(\lambda R_k) [Y_m(\lambda \rho_0) - iJ_m(\lambda \rho_0)] + \frac{2}{\pi} (-1)^{n-m} I_{n-m}(\lambda r_{k0}) I_n(\lambda R_k) K_m(\lambda \rho_0) \right\} \quad (31)$$

$$B_{mn}^k(\lambda \rho_0) = \frac{\pi R_k}{4\lambda D} e^{i(n-m)\theta_{k0}} \left\{ J_{n-m}(\lambda r_{k0}) J'_n(\lambda R_k) [Y_m(\lambda \rho_0) - iJ_m(\lambda \rho_0)] + \frac{2}{\pi} (-1)^{n-m} I_{n-m}(\lambda r_{k0}) I'_n(\lambda R_k) K_m(\lambda \rho_0) \right\} \quad (32)$$

By differentiating Eq. (28) with respect to ρ_0 , the slope θ near the circular boundary B_0 is given as

$$\theta(x; \rho_0, \phi_0) = \sum_{m=-M}^M e^{im\phi_0} \left\langle C_m^0(\lambda \rho_0) a_m^0 + D_m^0(\lambda \rho_0) b_m^0 - \sum_{k=1}^H \left[\sum_{n=-\infty}^{\infty} C_{mn}^k(\lambda \rho_0) a_n^k + \sum_{n=-\infty}^{\infty} D_{mn}^k(\lambda \rho_0) b_n^k \right] \right\rangle \quad (33)$$

where $C_m^0(\lambda \rho_0)$, $D_m^0(\lambda \rho_0)$, $C_{mn}^k(\lambda \rho_0)$, and $D_{mn}^k(\lambda \rho_0)$ can be obtained by differentiating $A_m^0(\lambda \rho_0)$, $B_m^0(\lambda \rho_0)$, $A_{mn}^k(\lambda \rho_0)$, and $B_{mn}^k(\lambda \rho_0)$ in Eqs. (29)–(32) with respect to ρ_0 .

Similarly, by applying the addition theorem to Eq. (22) and then using the moment operator of Eq. (7), the bending moment field $m(x)$ near the circular boundary B_p ($p=1, \dots, H$) can be expanded as follows:

$$m(x; \rho_p, \phi_p) = \sum_{m=-\infty}^{\infty} e^{im\phi_p} \left\langle E_m^p(\lambda \rho_p) a_m^p + F_m^p(\lambda \rho_p) b_m^p + \sum_{\substack{k=0 \\ k \neq p}}^H \varepsilon_k \left[\sum_{n=-\infty}^{\infty} E_{mn}^k(\lambda \rho_p) a_n^k + \sum_{n=-\infty}^{\infty} F_{mn}^k(\lambda \rho_p) b_n^k \right] \right\rangle \quad (34)$$

where $\varepsilon_k = -1$, $k=0$, and $\varepsilon_k = 1$, $k \neq 0$,

$$E_m^p(\lambda \rho_p) = \frac{\pi R_p}{4\lambda^2} \left\{ J_m(\lambda \rho_p) [\alpha_m^Y(\lambda \rho_p) - i\alpha_m^J(\lambda \rho_p)] + \frac{2}{\pi} I_m(\lambda \rho_p) \alpha_m^K(\lambda \rho_p) \right\} \quad (35)$$

$$F_m^p(\lambda \rho_p) = \frac{\pi R_p}{4\lambda} \left\{ J'_m(\lambda \rho_p) [\alpha_m^Y(\lambda \rho_p) - i\alpha_m^J(\lambda \rho_p)] + \frac{2}{\pi} I'_m(\lambda \rho_p) \alpha_m^K(\lambda \rho_p) \right\} \quad (36)$$

$$E_{mn}^k(\lambda \rho_p) = \begin{cases} \frac{\pi R_k}{4\lambda^2} e^{i(n-m)\theta_{kp}} \left\{ J_{n-m}(\lambda r_{kp}) \alpha_m^J(\lambda \rho_p) [Y_n(\lambda R_k) - iJ_n(\lambda R_k)] + \frac{2}{\pi} J_{n-m}(\lambda r_{kp}) \alpha_m^J(\lambda \rho_p) K_n(\lambda R_k) \right\}, & k=0 \\ \frac{\pi R_k}{4\lambda^2} e^{i(n-m)\theta_{kp}} \left\{ \alpha_m^J(\lambda \rho_p) J_n(\lambda R_k) [Y_{n-m}(\lambda r_{kp}) - iJ_{n-m}(\lambda r_{kp})] + \frac{2}{\pi} (-1)^m \alpha_m^J(\lambda \rho_p) I_n(\lambda R_k) K_{n-m}(\lambda r_{kp}) \right\}, & k \neq 0, p \end{cases} \quad (37)$$

$$F_{mn}^k(\lambda \rho_p) = \begin{cases} \frac{\pi R_k}{4\lambda} e^{i(n-m)\theta_{kp}} \left\{ J_{n-m}(\lambda r_{kp}) \alpha_m^J(\lambda \rho_p) [Y'_n(\lambda R_k) - iJ'_n(\lambda R_k)] + \frac{2}{\pi} J_{n-m}(\lambda r_{kp}) \alpha_m^J(\lambda \rho_p) K'_n(\lambda R_k) \right\}, & k=0 \\ \frac{\pi R_k}{4\lambda} e^{i(n-m)\theta_{kp}} \left\{ \alpha_m^J(\lambda \rho_p) J'_n(\lambda R_k) [Y_{n-m}(\lambda r_{kp}) - iJ_{n-m}(\lambda r_{kp})] + \frac{2}{\pi} (-1)^m \alpha_m^J(\lambda \rho_p) I'_n(\lambda R_k) K_{n-m}(\lambda r_{kp}) \right\}, & k \neq 0, p \end{cases} \quad (38)$$

where the moment operator $\alpha_m^X(\lambda \rho)$ from Eq. (7) is defined as

$$\alpha_m^X(\lambda \rho) = D \left\{ (1-\mu) \frac{X'_m(\lambda \rho)}{\rho} - \left[(1-\mu) \frac{m^2}{\rho^2} \mp \lambda^2 \right] X_m(\lambda \rho) \right\} \quad (39)$$

in which the upper (lower) signs refer to $X=J, Y$ (I, K), respectively. The differential equations for the Bessel's functions have been used to simplify $\alpha_m^X(\lambda \rho)$.

From Eq. (8), the effective shear operator $\beta_m^X(\lambda \rho)$ can be expressed as follows:

$$\beta_m^X(\lambda \rho) = D \left\{ [m^2(1-\mu) \pm (\lambda \rho)^2] \frac{X'_m(\lambda \rho)}{\rho^2} - m^2(1-\mu) \frac{X_m(\lambda \rho)}{\rho^3} \right\} \quad (40)$$

Similarly, the effective shear field $v(x)$ near the circular boundary B_p ($p=1, \dots, H$) can be expressed as follows:

$$v(x; p_p, \phi_p) = \sum_{m=-\infty}^{\infty} e^{im\phi_p} \left[G_m^p(\lambda\rho_p) a_m^p + H_m^p(\lambda\rho_p) b_m^p + \sum_{k=1}^H \varepsilon_k \left[\sum_{n=-\infty}^{\infty} G_{mn}^k(\lambda\rho_p) a_n^k + \sum_{n=-\infty}^{\infty} H_{mn}^k(\lambda\rho_p) b_n^k \right] \right] \quad (41)$$

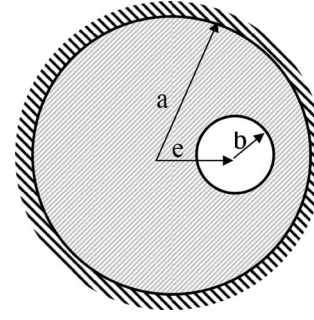
where $G_m^p(\lambda\rho_p)$, $H_m^p(\lambda\rho_p)$, $G_{mn}^k(\lambda\rho_p)$, and $H_{mn}^k(\lambda\rho_p)$ are obtained by replacing $\alpha_m^X(\lambda\rho_p)$ in Eqs. (35)–(38) by $\beta_m^X(\lambda\rho_p)$.

For an outer clamped circular plate ($u=\theta=0$) with multiple circular holes subject to free edge ($m=v=0$), by setting ρ_p to R_p and applying the orthogonal property of $\{e^{im\phi_p}\}$ ($p=0, 1, \dots, H$), Eqs. (28), (33), (34), and (41) yield

$$\begin{aligned} A_m^0(\lambda R_0) a_m^0 + B_m^0(\lambda R_0) b_m^0 - \sum_{k=1}^H \left[\sum_{n=-\infty}^{\infty} A_{mn}^k(\lambda R_0) a_n^k + \sum_{n=-\infty}^{\infty} B_{mn}^k(\lambda R_0) b_n^k \right] &= 0 \\ C_m^0(\lambda R_0) a_m^0 + D_m^0(\lambda R_0) b_m^0 - \sum_{k=1}^H \left[\sum_{n=-\infty}^{\infty} C_{mn}^k(\lambda R_0) a_n^k + \sum_{n=-\infty}^{\infty} D_{mn}^k(\lambda R_0) b_n^k \right] &= 0 \\ E_m^p(\lambda R_p) a_m^p + F_m^p(\lambda R_p) b_m^p + \sum_{k=0}^H \varepsilon_k \left[\sum_{n=-\infty}^{\infty} E_{mn}^k(\lambda R_p) a_n^k + \sum_{n=-\infty}^{\infty} F_{mn}^k(\lambda R_p) b_n^k \right] &= 0 \\ G_m^p(\lambda R_p) a_m^p + H_m^p(\lambda R_p) b_m^p + \sum_{k=0}^H \varepsilon_k \left[\sum_{n=-\infty}^{\infty} G_{mn}^k(\lambda R_p) a_n^k + \sum_{n=-\infty}^{\infty} H_{mn}^k(\lambda R_p) b_n^k \right] &= 0 \end{aligned} \quad (42)$$

for $m=0, \pm 1, \pm 2, \dots$, $n=0, \pm 1, \pm 2, \dots$, and $p=1, \dots, H$. Equation (42) results in a coupled infinite system of simultaneous linear algebraic equations for the coefficients a_m^k and b_m^k , $k=0, \dots, H$.

For an outer free circular plate ($m=v=0$) with multiple circular holes subject to a clamped edge ($u=\theta=0$), a coupled infinite system of linear equations analogous to Eq. (42) can be similarly obtained as follows: (1) $A_m^0(\lambda R_0)$, $B_m^0(\lambda R_0)$, $A_{mn}^k(\lambda R_0)$, and $B_{mn}^k(\lambda R_0)$ in Eq. (42) are determined by replacing $X_m(\lambda\rho_0)$ in Eqs. (29)–(32) with $\alpha_m^X(\lambda\rho_0)$ and setting ρ_0 to R_0 , where the notation X represents J , Y , I , and K , respectively; (2) $C_m^0(\lambda R_0)$, $D_m^0(\lambda R_0)$, $C_{mn}^k(\lambda R_0)$, and $D_{mn}^k(\lambda R_0)$ in Eq. (42) can be similarly obtained, but here $\beta_m^X(\lambda\rho_0)$ is used; (3) $E_m^p(\lambda R_p)$, $F_m^p(\lambda R_p)$, $E_{mn}^k(\lambda R_p)$, and $F_{mn}^k(\lambda R_p)$ in Eq. (42) are determined by replacing $\alpha_m^X(\lambda\rho_0)$ in Eqs. (35)–(38) with $X_m(\lambda\rho_0)$ and setting ρ_0 to R_0 ; and (4) differentiating the coefficients in (3) with respect to ρ_0 and setting ρ_0 to R_0 yield $G_m^p(\lambda R_p)$, $H_m^p(\lambda R_p)$, $G_{mn}^k(\lambda R_p)$, and $H_{mn}^k(\lambda R_p)$ in Eq. (42).



Case 1:

Geometric data:
 $a=1\text{m}$
 $b=0.25\text{m}$
 $e=0.45\text{m}$
thickness=0.002m
Boundary condition:
Inner circle : free
Outer circle: clamped

Fig. 4 A circular plate with an eccentric hole subject to clamped-free boundary conditions

In the following computation, only the finite M terms are used in Eq. (42). Based on the direct-searching scheme [12], the natural frequencies are determined as the minimum singular value from the SVD of the truncated finite system by performing the frequency sweep. In our approach, two steps are employed. In the first step, the larger frequency interval $\Delta\lambda$ is taken. For example,

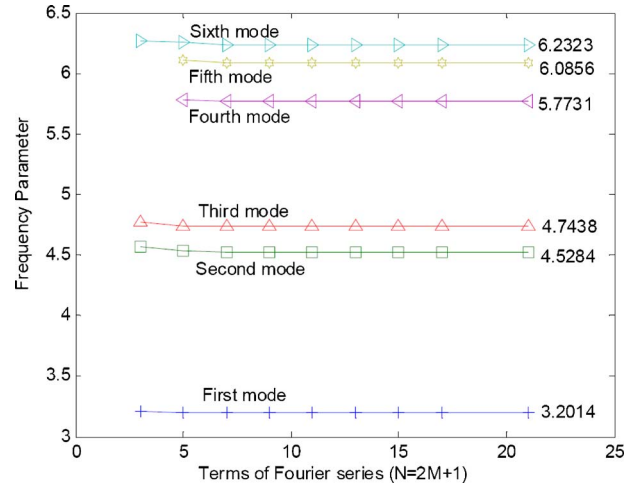


Fig. 5 Natural frequency parameter versus the number of terms of Fourier series for a circular plate with an eccentric hole ($a=1.0$, $b=0.25$, $e/a=0.45$)

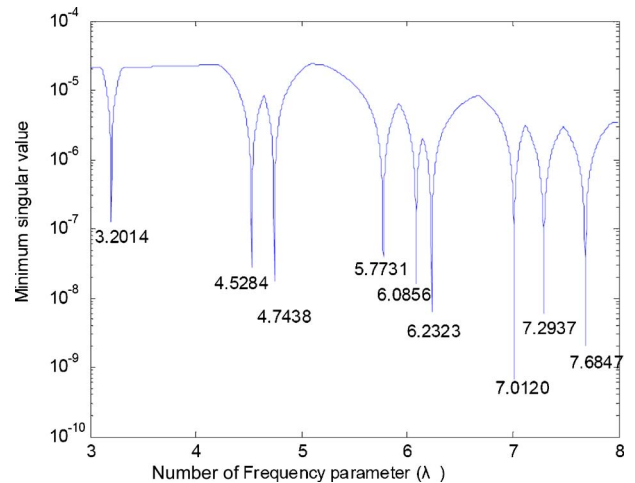


Fig. 6 The minimum singular value versus the frequency parameter for a circular plate with one eccentric hole ($a=1.0$, $b=0.25$, $e=0.45$)

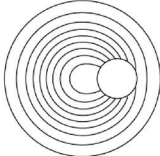
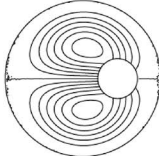
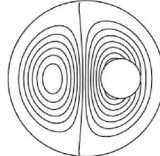
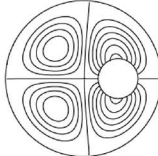
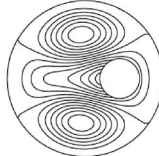
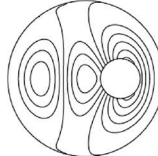
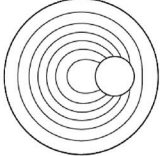
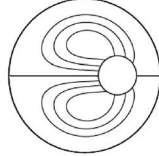
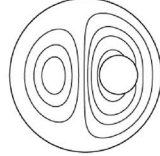
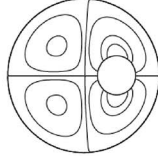
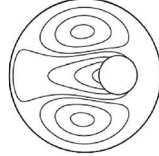
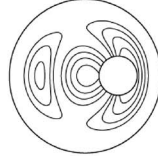
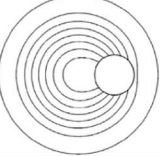
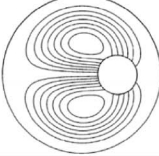
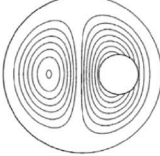
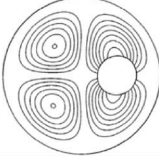
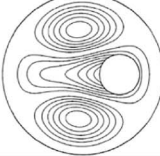
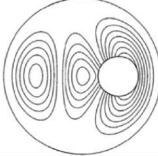
Mode No.	1	2	3	4	5	6
Approach	3.2014	4.5284	4.7438	5.7731	6.0856	6.2323
Present method						
	3.1870	4.5210	4.7400	5.7580	6.0600	6.2560
Semi-analytical method [10]						
	3.2014	4.5274	4.7439	5.7723	6.0841	6.2333
ABAQUS						

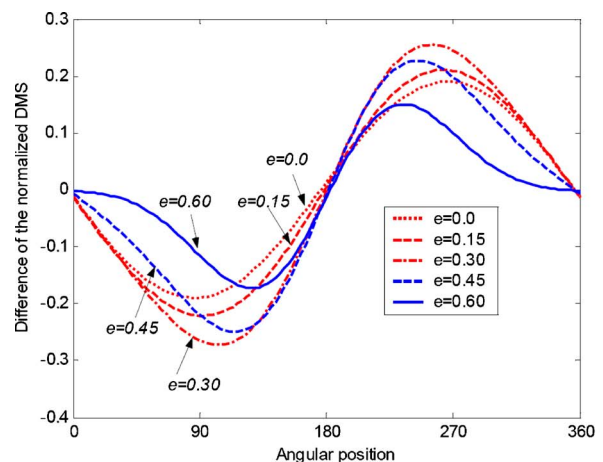
Fig. 7 The lower six natural frequency parameters and modes of a circular plate with an eccentric hole ($a=1.0$, $b=0.25$, $e=0.45$)

the value of 0.1 is chosen to sweep the frequency range of our concern. For the second step, the local sweep with the smaller one proceeded depending on the precision requirement of the considered problem. For instance, the value of 0.0001 is adopted in this paper. That is to say, the adaptive scheme of $\Delta\lambda$ is used. Once the eigenvalues are found, the associated mode shapes can be obtained by substituting the corresponding boundary eigenvectors (i.e., the complex Fourier series representing the fictitious boundary density) into the boundary integral equations.

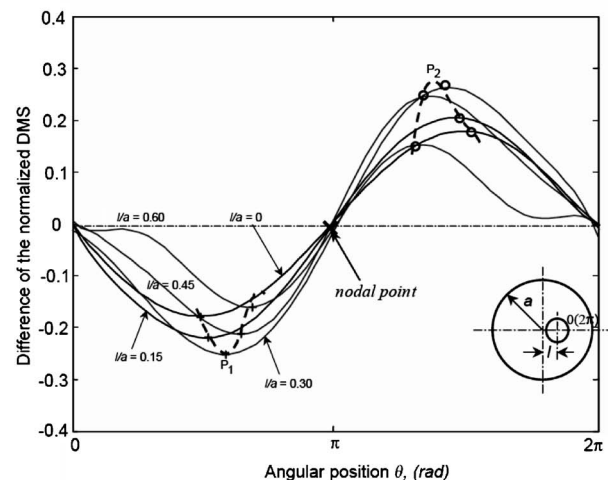
4 Numerical Results and Discussions

To demonstrate the proposed method, the FORTRAN code was implemented to determine natural frequencies and modes of a circular plate with multiple circular holes. The same problem was independently solved by using FEM (the ABAQUS software) for comparison. In all cases, the inner boundary is subject to the free boundary condition, the thickness of the plate is 0.002 m, and the Poisson's ratio μ is 1/3 unless otherwise specified. The general-purpose linear triangular elements of type S3 were employed to model the plate problem by using ABAQUS. Although the thickness of the plate is 0.002 m, these elements do not suffer from the transverse shear locking based on the theoretical manual of ABAQUS [14].

4.1 Case 1: A Circular Plate With an Eccentric Hole [2,10]. A circular plate with an eccentric hole, as shown in Fig. 4, is considered. The outer and inner radii are 1 m ($R_1=1$ m) and 0.25 m ($R_2=0.25$ m), respectively, and the offset distance e for the eccentric hole is 0.45 m ($e/a=0.45$). The lower six natural frequency parameters versus the number of terms of Fourier series N are shown in Fig. 5. It shows that the proposed solution promptly converges by using only a few terms of Fourier series. In addition, only the fourth and fifth modes are lost in the former six modes when M equals to 1. The convergence rate is superior to that by using the collocation approach [10] for the same problem. Figure 6 indicates the minimum singular value of the influence matrix versus the frequency parameter λ when using 11 terms of Fourier series ($N=11$). Since the direct-searching scheme is used, the drop location indicates the eigenvalue. The FEM was employed to solve the same problem, and its model has 242,211 elements and 121,891 nodes in order to obtain acceptable results for comparison. The lower six natural frequency parameters and



(a) the present method



(b) the Finite element method

Fig. 8 Contour of residual DMSs around the hole with eccentricity e from 0 to 0.6: (a) the present method and (b) the finite element method [8]

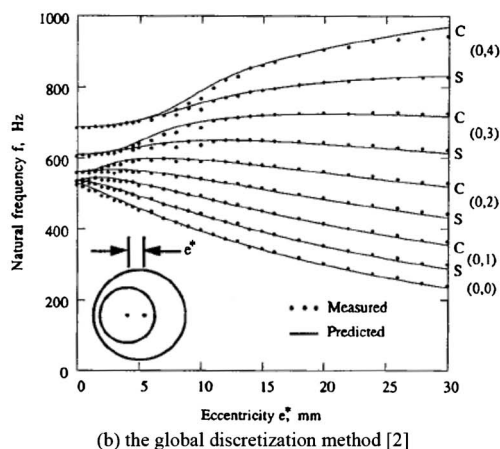
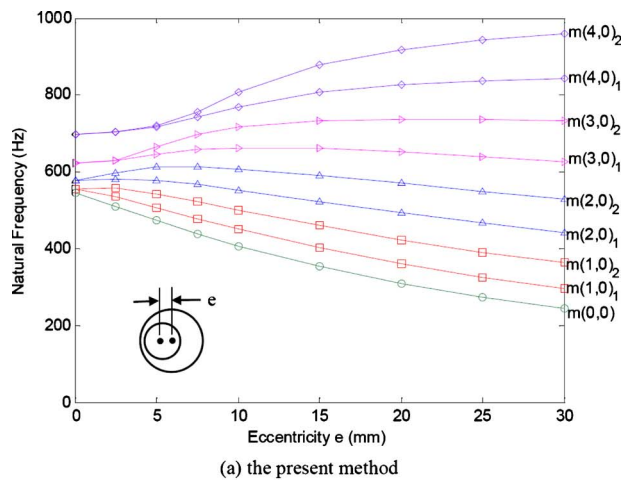


Fig. 9 Effect of the eccentricity e on the natural frequencies for the free-clamped annular-like plate: (a) the present method and (b) the global discretization method [2]

modes by using the present method, the semi-analytical method [10], and FEM are shown in Fig. 7. The results of the present method match well with those of FEM by using the ABAQUS. It indicates that the semi-analytical results show some deviations from the other results due to the complicated transformation of the effective shear force.

It may be worth mentioning that the proposed method can perform a local vibration analysis by using the residual displacement mode shape (DMS), defined as the difference of DMS between the circular and annular-like plate to the problem of damage detection [8]. Figure 8 shows the contour of residual DMSs of mode (1,0) [10] around the hole with eccentricity e from 0 to 0.6 by using (a)

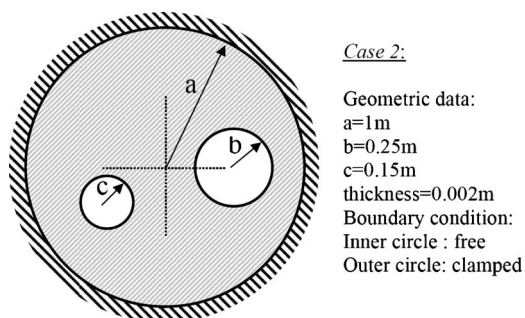


Fig. 10 A circular plate with two holes subject to clamped-free boundary conditions

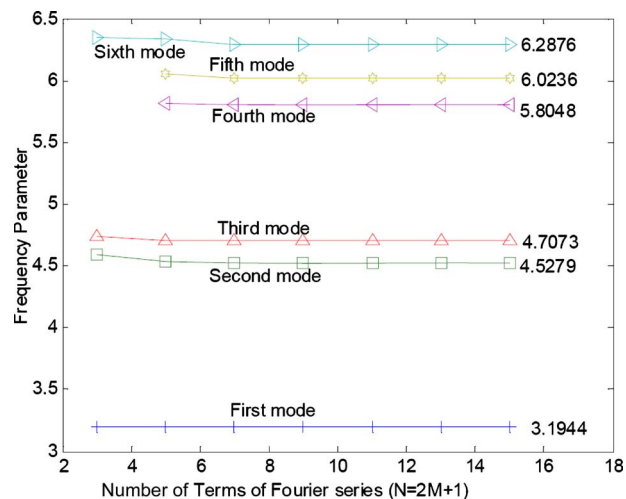


Fig. 11 Natural frequency parameter versus the number of terms of Fourier series for a circular plate with two holes ($a=1.0$, $b=0.25$, $c=0.15$)

the present method and (b) the finite element method [8]. The unobvious change around the hole in the DMS, even for a small eccentricity, can be detected clearly from the residual DMS analysis. It can provide an approach to identify damage occurring in the annular-like plate.

The next example is a commercial computer hard disk drive [2], which is an annular aluminum plate. The outer and inner radii are 178 mm and 84 mm, respectively, and the thickness is 1.9 mm. The plate was fixtured between two solid circular aluminum flanges with an outside radius of 124 mm. The flanges were aligned and positioned on the plate at a specified value of e within the range of 0–30 mm. Figure 9 is the effect of the eccentricity e on the natural frequencies for the free-clamped annular-like plate by using (a) the present method and (b) the global discretization method. Good agreement can be observed. Values of m and n in the mode (m,n) [10] shown in Fig. 9 are numbers of diametrical nodal lines and circular nodal lines, respectively. Subscript 1 denotes the straight diametrical nodal line, while subscript 2 denotes the curved diametrical nodal line [10]. It shows that an annular-like plate with small eccentricity has close eigenfrequencies and is apt to result in beating between those close eigenmodes.

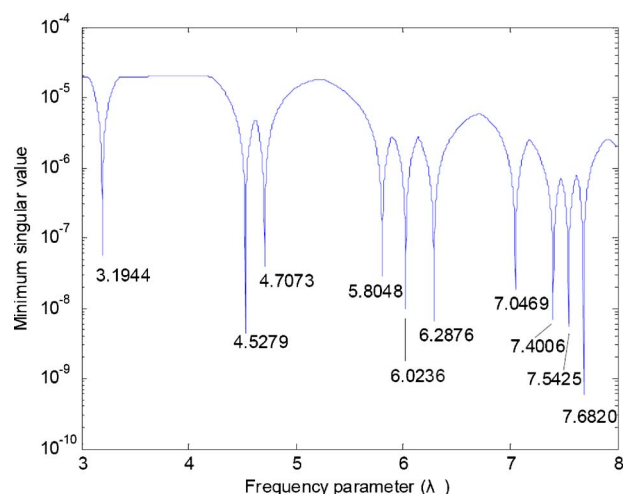


Fig. 12 The minimum singular value versus the frequency parameter for a circular plate with two holes ($a=1.0$, $b=0.25$, $c=0.15$)

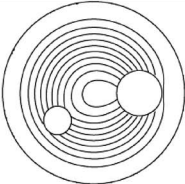
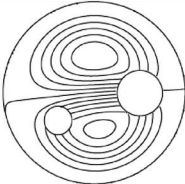
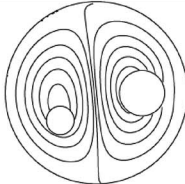
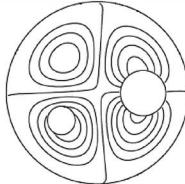
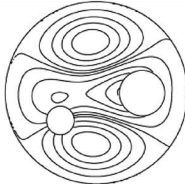
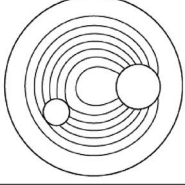
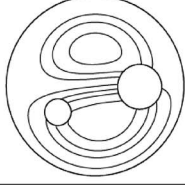
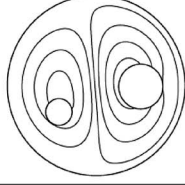
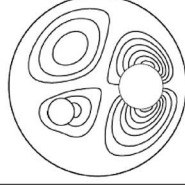
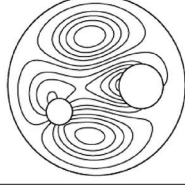
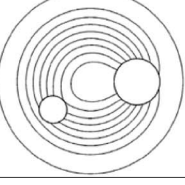
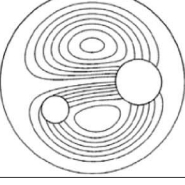
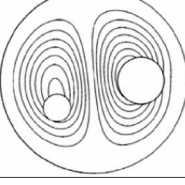
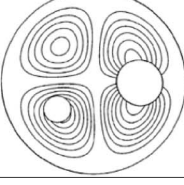
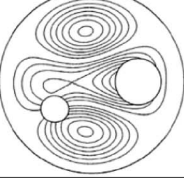
Mode No. Approach	1	2	3	4	5
	3.1944	4.5279	4.7073	5.8048	6.0236
Present method					
Semi-analytical method [10]	3.1770	4.5290	4.699	5.7510	5.9570
					
ABAQUS	3.1943	4.5270	4.7089	5.8062	6.0222
					

Fig. 13 The lower five natural frequency parameters and modes of a circular plate with two holes ($a=1.0$, $b=0.25$, $c=0.15$)

4.2 Case 2: A Circular Plate With Two Holes [10]. In order to demonstrate the generality of the present method, a circular plate with two holes is considered, as shown in Fig. 10. The radii of holes are 0.25 m and 0.15 m, and the coordinates of the centers are (0.5, 0.0) and (−0.4, −0.3), respectively. The lower six natural frequency parameters versus the number of terms of Fourier series N are shown in Fig. 11. When the number of inner circular hole increases, the fast convergence rate can also be observed. The sixth mode shows a slower convergence rate due to the complex geometrical configuration. Figure 12 indicates the minimum singular value of the influence matrix versus the frequency parameter λ when using 11 terms of Fourier series ($N=11$). To achieve a comparable solution for comparison, the FEM needs 136,670 elements. The lower five natural frequency parameters and modes by using the present method, the semi-analytical method [10], and the FEM are shown in Fig. 13. Good agreement between the results of the present method and those of the ABAQUS is observed.

To investigate the hole-hole interaction [18], a circular plate containing two identical holes with different central distances is studied. The radii of the circular plate and the circular hole are 1 m and 0.15 m, and the dimensionless distances of two holes L/a are chosen as 2.1, 2.5, and 4.0 in the numerical experiments, where a is the radius of circular holes and L is the central distance of two holes. Numerical results show that the space of two holes has a minor effect on the lower eigenfrequencies. Regarding eigenmodes shown in Fig. 14, the zone of the maximum deformation, enclosed with the dashed line, for the case of $L/a=2.1$ is significantly less than that for $L/a=4.0$. Consequently, the dynamic stress concentration [19] for the case of $L/a=2.1$ is larger because the distortion energy caused by the external loading concentrates in the smaller area.

Our proposed method has advantages over both the analytical methods and the numerical methods, such as the conventional BEM or the FEM. On one hand, it is clearly convinced that the proposed formulation is applicable to problems with multiple circular holes, which cannot be solved easily by the other analytical methods. On the other hand, it is demonstrated that the proposed method has advantages, such as the good accuracy and fast rate of convergence over the conventional BEM or FEM.

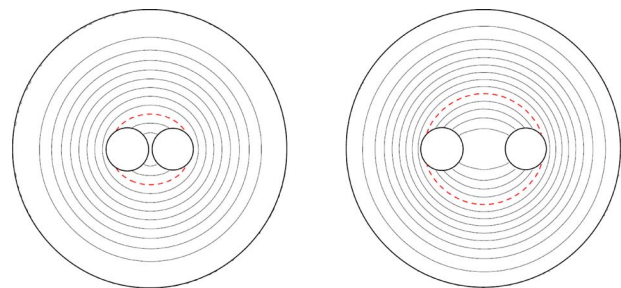


Fig. 14 The first natural frequency parameters and modes of a circular plate with two holes: (a) $L/a=2.1$ and (b) $L/a=4.0$

5 Concluding Remarks

An analytical model for the free vibration of a circular plate with multiple circular holes was derived as a coupled infinite system of simultaneous linear algebraic equations. Natural frequencies and natural modes of the stated problem were determined in the truncated finite system by using the direct-searching scheme. The proposed method utilized indirect boundary integral equations, the addition theorem, and the complex Fourier series. Owing to the addition theorem, two critical problems of improper integration in the indirectly connected domain problems were successively solved in a novel way. The proposed results match well with those provided by FEM using a lot of elements to obtain acceptable solutions for comparison. It shows good accuracy and fast rate of convergence, thanks to the analytical approach. Besides, the proposed numerical results have attempted explanations for the beating in the rotating machinery and the dynamic stress concentration when two holes are close to each other.

Acknowledgments

Financial support from the National Science Council under the Grant No. NSC-98-2221-E-157 and NSC-97-2221-E-019-015-

References

- [1] Khurasia, H. B., and Rawtani, S., 1978, "Vibration Analysis of Circular Plates With Eccentric Hole," *ASME J. Appl. Mech.*, **45**, pp. 215–217.
- [2] Tseng, J. G., and Wickert, J. A., 1994, "Vibration of an Eccentrically Clamped Annular Plate," *ASME J. Appl. Mech.*, **116**, pp. 155–160.
- [3] Leissa, A. W., and Narita, Y., 1980, "Natural Frequencies of Simply Supported Circular Plates," *J. Sound Vib.*, **70**, pp. 221–229.
- [4] Vogel, S. M., and Skinner, D. W., 1965, "Natural Frequencies of Transversely Vibrating Uniform Annular Plates," *ASME J. Appl. Mech.*, **32**, pp. 926–931.
- [5] Vega, D. A., Vera, S. A., Sanchez, M. D., and Laura, P. A. A., 1998, "Transverse Vibrations of Circular, Annular Plates With a Free Inner Boundary," *J. Acoust. Soc. Am.*, **103**, pp. 1225–1226.
- [6] Vera, S. A., Sanchez, M. D., Laura, P. A. A., and Vega, D. A., 1998, "Transverse Vibrations of Circular, Annular Plates With Several Combinations of Boundary Conditions," *J. Sound Vib.*, **213**(4), pp. 757–762.
- [7] Vera, S. A., Laura, P. A. A., and Vega, D. A., 1999, "Transverse Vibrations of a Free-Free Circular Annular Plate," *J. Sound Vib.*, **224**(2), pp. 379–383.
- [8] Cheng, L., Li, Y. Y., and Yam, L. H., 2003, "Vibration Analysis of Annular-Like Plates," *J. Sound Vib.*, **262**, pp. 1153–1170.
- [9] Laura, P. A. A., Masia, U., and Avalos, D. R., 2006, "Small Amplitude, Transverse Vibrations of Circular Plates Elastically Restrained Against Rotation With an Eccentric Circular Perforation With a Free Edge," *J. Sound Vib.*, **292**, pp. 1004–1010.
- [10] Lee, W. M., Chen, J. T., and Lee, Y. T., 2007, "Free Vibration Analysis of Circular Plates With Multiple Circular Holes Using Indirect BIEMs," *J. Sound Vib.*, **304**, pp. 811–830.
- [11] Providakis, C. P., and Beskos, D. E., 1999, "Dynamic Analysis of Plates by Boundary Elements," *Appl. Mech. Rev.*, **52**(7), pp. 213–236.
- [12] Kitahara, M., 1985, *Boundary Integral Equation Methods in Eigenvalue Problems of Elastodynamics and Thin Plates*, Elsevier, Amsterdam.
- [13] IMSL, 1999, *Math/Library Volumes 1 and 2*, Version 4.01, Visual Numerics, Inc.
- [14] ABAQUS 6.5, 2004, Hibbitt, Karlsson and Sorensen, Inc., RI.
- [15] Nagaya, K., and Poltorak, K., 1989, "Method for Solving Eigenvalue Problems of the Helmholtz Equation With a Circular Outer and a Number of Eccentric Circular Inner Boundaries," *J. Acoust. Soc. Am.*, **85**, pp. 576–581.
- [16] Watson, G. N., 1995, *A Treatise on the Theory of Bessel Functions*, 2nd ed., Cambridge Library, Cambridge.
- [17] Martin, P. A., 2006, *Multiple Scattering Interaction of Time-Harmonic Wave With N Obstacles*, Cambridge University Press, Cambridge.
- [18] Chandra, A., Huang, Y., Wei, X., and Hu, K. X., 1995, "A Hybrid Micro-Macro BEM Formulation for Micro-Crack Clusters in Elastic Components," *Int. J. Numer. Methods Eng.*, **38**(7), pp. 1215–1236.
- [19] Lee, W. M., and Chen, J. T., 2008, "Scattering of Flexural Wave in Thin Plate With Multiple Holes by Using the Null-Field Integral Equation Approach," *Comput. Model. Eng. Sci.*, **1124**(1), pp. 1–30.